Spatially Resolved Anisotropic Natural Abundance Deuterium 2D-NMR Spectroscopy Using Bimesophasic Lyotropic Chiral Systems

Thomas Julien, Boris Gouilleux, Bernard Rousseau, Stefan Immel, Michael Reggelin, Philippe Lesot

Spatially Resolved Anisotropic Natural Abundance Deuterium 2D-NMR Spectroscopy using Bimesophasic Lyotropic Chiral Systems

Thomas Julien,[a] Boris Gouilleux,[a] Bernard Rousseau,[a,b] Stefan Immel,[c] Michael Reggelin*[c] and Philippe Lesot*[a,b]

[a] RMN en Milieu Orienté, Institut de Chimie moléculaire et des Matériaux d'Orsay (ICMMO), UMR 8182, Université Paris-Saclay, UFR des Sciences d'Orsay,
17-19, Avenue des Sciences, F-91400 Orsay, France.
[b] Centre National de la Recherche Scientifique (CNRS),
3, Rue Michel Ange, F-75016 Paris, France.
[c] Clemens-Schöpf-Institut für Organische Chemie und Biochemie Technische Universität Darmstadt,
Peter Grünberg-Strasse 4, 64287 Darmstadt, Germany.

Corresponding Authors
E-mail: philippe.lesot@universite-paris-saclay.fr
E-mail: re@chemie.tu-darmstadt.de

ORCID :

Philippe Lesot : orcid.org/0000-0002-5811-7530
Michael Reggelin : orcid.org/0000-0003-3650-3921
Boris Gouilleux : orcid.org/0000-0002-6491-3525
Bernard Rousseau : orcid.org/0000-0001-7096-9069
Stefan Immel : orcid.org/0000-0002-6524-2399

ABSTRACT:
In this communication, we describe, for the first time, the combined and original use of spatially-resolved anisotropic natural abundance deuterium (ANAD) 2D-NMR experiments and bimesophasic lyotropic chiral systems to extract two independent sets of anisotropic parameters such as ^{2}H-RQCs from a single NMR sample. As pioneering example, we focus on a mixture of immiscible polypeptides (PBLG) and polyacetylene helical polymers (L-MSP) dissolved in weakly polar organic solvents (chloroform). Non-deuterated (D)-(+)-camphor is used as a model chiral solute. By providing two series of ^{2}H-RQCs, this new analytical approach paves the way for applications in 3D structure elucidation with increased reliability, and also opens up original investigations in terms of spectral enantiomeric discriminations and mixing of helical polymers.

KEYWORDS:
Lyotropic bimesophasic systems, Localized NMR spectroscopy, Deuterium 2D NMR, Residual quadrupolar coupling, Structural analysis.

MAIN TEXT:

Weakly orienting systems (lyotropic liquid crystals (LLCs) or aligning media (as compressed/stretched gels)) have widened analytical possibilities of anisotropic NMR in the frame of the molecular analysis, especially when chirality is involved.[1] Various NMR methodological developments involving residual chemical shift anisotropy (RCSA), residual dipolar coupling (RDC) and residual quadrupolar coupling (RQC) have been proposed to solve various challenges faced by chemists in the frame of 3D structural determination of small synthesized molecules or natural compounds.[2,3,4]

As any other anisotropic interaction (RDCs or RCSAs), ^{2}H-RQCs (measured with spins $I > ½$) can be related to Saupe's order matrix, $S_{\alpha\beta}$, (or alignment tensor, $A_{\alpha\beta} = \frac{2}{3}S_{\alpha\beta}$) that encodes a geometrical information associated with a molecule:[5,6]

$$\frac{2}{3}\frac{\Delta\nu_{Q_i}^{\text{Exptl.}}}{QCC_{CD_i}} = \sum_{\alpha,\beta=a,b,c} \cos\theta_{CD_i}^{\alpha} \cos\theta_{CD_i}^{\beta} S_{\alpha\beta} \quad (1)$$

where QCC_{CDi} is the ^{2}H quadrupolar coupling constant and $\theta_{CD_i}^{\alpha\ or\ \beta}$ are the cosine directors defined as the angle between a C-D_i bond and the a, b, c axes of the molecular axis frame.

In practice, it can be of interest to determine anisotropic data (RCSAs, RDCs or RQCs or their combination) in more than one ordered solvent to increase the reliability of a structural assignment,[7,8,9] to reduce the number of predetermined structural information or for the purpose of structure refinements (*e.g.* the treatment of conformational flexibility of analytes).[10,11,12,13,14] As an alternative to historical, monomesophasic chiral LLCs, it has recently been reported the concept of polymer-based thermoresponsive lyotropic systems which provide two different types of aligning environments at two different temperatures due to a significant molecular reorganization of the polymer (or possibly the phase director) in the NMR sample leading to independent anisotropic data usable for structure elucidation purposes.[15,16]

In this work, we explore a novel concept which consists to prepare in one NMR tube two immiscible polymeric based chiral LLCs in order to obtain, after the demixing process, two uniform and homogenous chiral mesophases. Each of them exhibits its own orientation properties while being stable over time and clearly identified by a discernible LLC/LLC interface.[17] As first pioneering and illustrative example, we present the case of "chiral bimesophasic mixtures" made of a well-known polypeptide polymer (PBLG)[1] and a more recent polyacetylene polymer (L-MSP)[18] whose molecular structures are shown in **Scheme 1**.

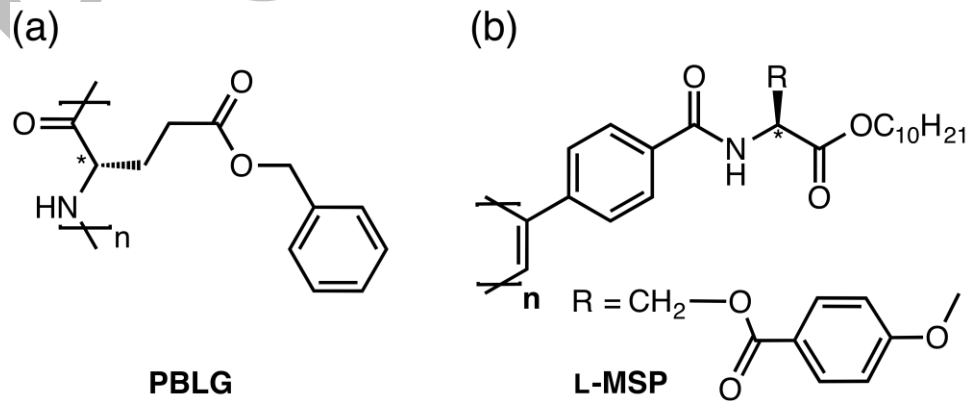

Scheme 1. Molecular structure of (a) PBLG and (b) L-MSP helically chiral polymer.

The protocol for the preparation bimesophasic-sample does not differ from that used for preparing the conventional polypeptide- or polyacetylene-based LLCs samples, the only difference being the addition of two polymers instead of one (in adapted quantities). All mixture ingredients are weighted directly into the NMR tube (5-mm o.d.), which is then fire-sealed. A series of centrifugations to homogenise both phases is necessary after the initial sample preparation. Then, as long as the spectral resolution is acceptable, there is no need to rehomogenise the bimesophasic samples (by centrifugation) between series of experiments. Details are given in **SI**. At the end of the demixing process, when the LLC/LLC interface is visible (see **Figure 1**), the alignment properties of each nematic phase can be evaluated using ^{2}H z-imaging 2D experiments on the $CDCl_3$ signal.[19]

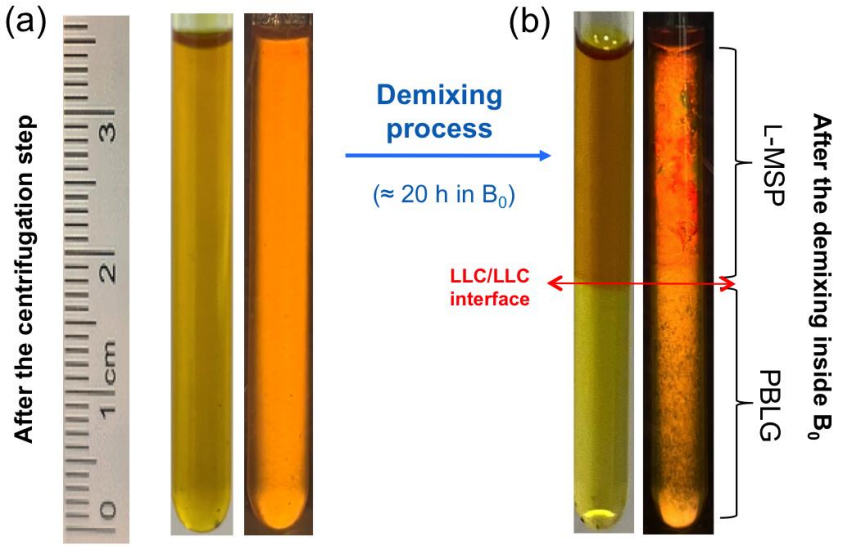

Figure 1. Images of the NMR tube made of PBLG/L-MSP/$CH(D)Cl_3$: (a) just after sample centrifugation and observed without (left) and with a polarised light (right), (b) after the demixing in B_0 when the mesophase interface is visible (with or without polarised light). Here two uniform birefringent domains are observed.

Figure 2 shows a typical example of a ^{2}H z-imaging 2D map when the PBLG (bottom) and L-MSP (top) polymers are clearly separated and located into two distinct regions of the NMR tube (no signal overlap on the z-dimension) and leads to two well-resolved ^{2}H-QDs with different $\Delta\nu_Q^{PBLG}{}_{^2H} \neq \Delta\nu_Q^{L-MSP}{}_{^2H}$. This ^{2}H z-imaging experiment on a deuterated solute allows to check two key aspects of the sample alignment: i) each chiral mesophase is uniformly oriented in $\boldsymbol{B}_0$ (both components of the ^{2}H-QD are parallel to each other with the same splitting along z), and ii) the solute is homogeneously aligned (no tilting, distortion or incurvation of the QD components) along z.

From a methodological point of view, ^{2}H NMR of two demixed mesophases consists to record selectively the ^{2}H spectrum of the solute (deuterated or at natural abundance deuterium (NAD) level) for each phase (lower and upper layer along the z-axis) with the aim to extract two independent datasets of ^{2}H-RQCs. For performing spatially resolved NMR experiments on bimesophasic samples, we adopted the selective saturation of volumes surrounding the region of interest, known as Outer Volume Suppression (OVS), that relies on the concurrent use of magnetic field gradients and selective pulses to saturate the targeted sample region.[20,21] Applied to ^{2}H NMR in anisotropic samples, the "OVS" approach is advantageous because this suppression block is easy to implement in any *n*D NMR pulse sequence, as it is generally performed during the experiment preparation period. In addition, the magnetization located in the volume of interest is only subjected to hard pulses in contrast to the direct selection approach.[22] This avoids phase distortions that might occur from residual quadrupolar coupling

modulation during the application of selective pulses. The thickness Δz and the position z_0 of the slice to be saturated are defined by the bandwidth (BW) and the offset (Spoffs) of the selective pulse and the amplitude of the gradient (G) along z-axis.[20,21] Following the OVS block, any 1D or 2D experiment can be implemented as depicted in **Figure 3**. Combined together, we can selectively record the ^{2}H or NAD 1D or 2D spectra corresponding to the upper and lower phase of the sample (see the **SI**). The basic principle of OVS experiments is to eliminate the NMR signal from the unwanted regions (volumes) of the sample. In the case of demixed samples with two separate regions of almost equal length (top and bottom parts), it is relevant to centre the B_1 coil of the probe on the centre of the sample in order to maximize the spin density detected by each OVS *n*D NMR experiment (OVS1 and OVS2).

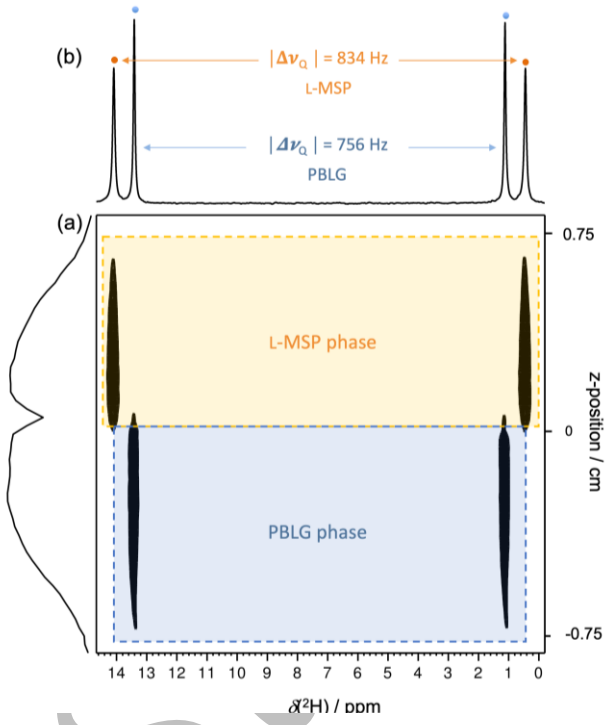

Figure 2. (a) Example of 61.4 MHz ^{2}H z-imaging 2D map (magnitude mode) of $CDCl_3$ in PBLG/L-MSP/$CHCl_3$ mixture (295 K) where two sets of ^{2}H signals are visible; the interfacial zone appears at the center. (b) The F_2 projection shows the ^{2}H 1D spectrum of the whole sample after demixing (see **Figure 1**). Details on the phase-encoding imaging experiment and parameters are given in **SI**.

Applying to bimesophasic mixtures (PBLG/L-MSP/$CHCl_3$), we have explored the capacity to record spatially-resolved ANAD-{^{1}H} QUOSY 2D experiments of small chiral molecules, and then exploit the ^{2}H-RQC data to determine the Saupe order matrix in each domain. As test molecule we used (D)-(1*R*, 4*R*)-(+)-camphor (noted **(D)-1**), a rigid bicyclic chiral solute displaying 10 non-equivalent hydrogen sites (see **Figure 4**). A priori, 10 ^{2}H-RQCs associated with 10 monodeuterated diastereo-isotopomers are expected to be measured in each mesophase. The identification of 10 ^{2}H-QDs expected for each nematic region (PBLG and L-MSP domain) is achieved by analyzing spatially-resolved ANAD-{^{1}H} phased *Q*-resolved 2D experiments in both regions (**Figures 4a** and **4b**), while the measurement of $\Delta\nu_Q^{Exptl.}$'s was made on the whole sample to avoid any experimental bias such as temperature variation) (see **Figure SI-9**). Note that the signal-to-noise ratio (SNR) measured on each ^{2}H-QD observed varies from ~3 to ~40.

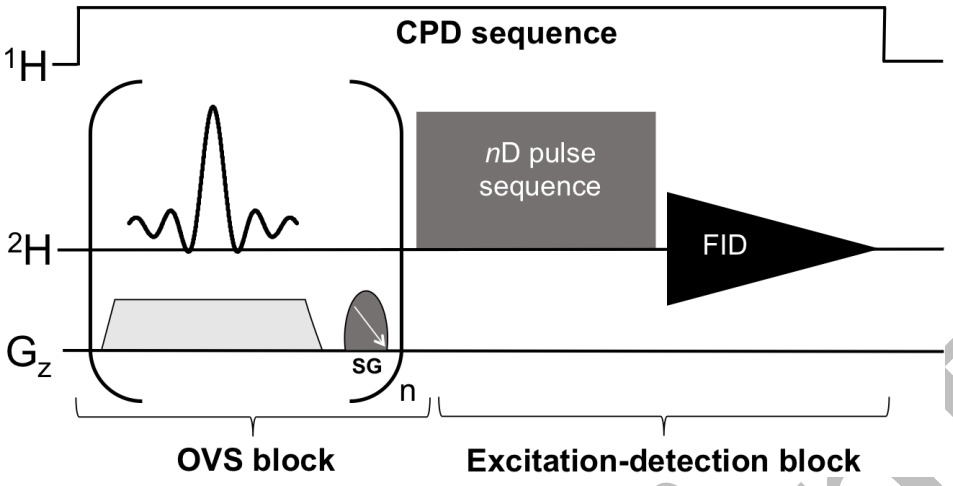

Figure 3. Principle of the spatially resolved ^{2}H-{^{1}H} *n*D NMR experiments using an OVS block. The minimal number of loop, n, for suppression, is 4 but can be larger. A sneeze-shaped selective pulse is used. The amplitude of spoiling gradient (SG) can vary through the loop n. The excitation-detection block can be a simple 1D sequence (90°-Acq.) or a multiple-pulse 2D sequence (QUOSY-type) (see the **SI**).

Due to the absence of conformational flexibility of camphor (bicylic molecule), the single-tensor approximation approach suffices for a robust configurational analysis.[23] Calculations are performed using the program ConArch^{+} 3.00i.[13] A structural model of **(D)-1** and the associated EFG tensor are determined by DFT (see **Table SI-3**) using the Gaussian 16, Rev.B software (*-vide infra-*). All experimental and back-calculated ^{2}H-RQC data ($\Delta\nu_Q(^2H)^{Exptl.}$ and $\Delta\nu_Q(^2H)^{Calc.}$) as well as all pertinent spectral ^{2}H data for **(D)-1** oriented in each mesophasic domain are listed in **Tables SI-4** and **SI-5**.

The signs of ^{2}H-RQCs used to calculate the Saupe matrix parameters originate from data reported in 2022 in the case of a scalemic mixture of camphor (*ee*(D) = 30%) dissolved separately in two monophasic samples of L-MSP and PBLG ($W_{Polym.}/W_{tot} \approx 19$ %).[18] This mass fraction of the polymer is in fact almost identical to that calculated in each domain of the bimesophasic sample, assuming an equal distribution (50%) of the analyte, polymer and co-solvent in the N^*_I and N^*_{II} mesophases ($[W_{Polym.\ I\ or\ Polym.\ II}]/[0.5*W_{tot}] = 19.2$ %).

The very small value of *Q*-factor and RMSD (0.015 and 2.24 Hz respectively) calculated on the set of 10 RQCs in the L-MSP domain indicates an excellent fit between the $\Delta\nu_Q(^2H)^{Exptl.}$ and $\Delta\nu_Q(^2H)^{Calc.}$ when the (1*R*,4*R*)-configuration is considered. In the case of data measured in the PBLG domain, we found initially an *Q*-factor of 0.064, but a surprisingly large RMSD value of 27 Hz ($|\Delta\Delta_Q(^2H)^{max}| = 55$ Hz) that possibly suggest an uncorrect sign for one or several RQCs.

The sign permutation (sign inversion) of all ^{2}H-RQCs (option available with the ConArch+ program)[13, 14] clearly shows that the sign of the ^{2}H-RQC at the position 6ex is negative instead of positive, leading to a lower *Q*-factor of 0.012 and an acceptable RMSD (4.96 Hz). The negative sign was confirmed by excluding the ^{2}H-RQC (6ex) from input data (9 ^{2}H-RQCs) resulting in a negative back-calculated RQC for this ^{2}H site, and experimentally corroborated by the analysis of the ^{13}C-^{1}H spectral pattern of carbon at 6-position (details are shown in the **SI**, **Figure SI-9**).

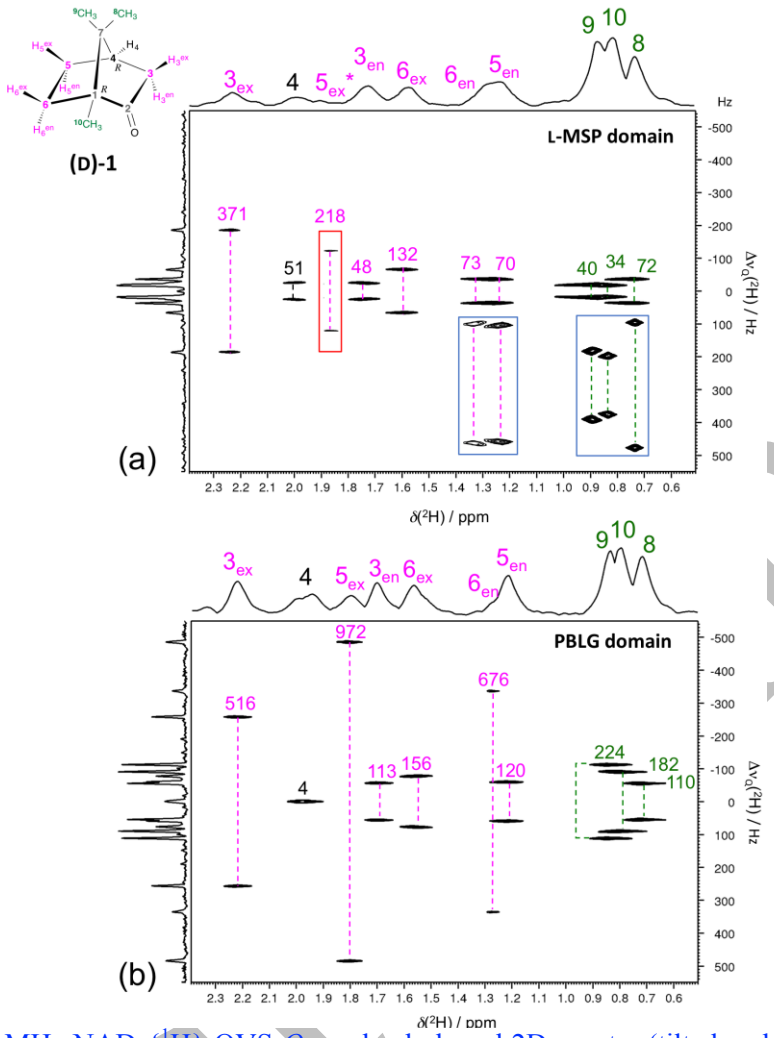

Figure 4. (a and b) 92.1 MHz NAD-{^{1}H} OVS *Q*-resolved phased 2D spectra (tilted and symmetrized) of **(D)-1** in the L-MSP/$CHCl_3$ and PBLG/$CHCl_3$ domain (297 K) along with the magnitude of quadrupolar splitting $\Delta\nu_Q(^2H)$ in Hz. 2D maps were acquired with 1840(t_2) × 280(t_1) data points (zerofilled to 4k × 4k), 224 scans per t_1 increment and a recycling delay of 0.6 s. Two zooms (blue boxes) are displayed in (a). The signal of the 5_{ex} deuteron exhibits a very low SNR (~3) and the associated contour levels shown (red inset) was adjusted by a factor of 2.

This result points out the interest to evaluate the quality of fits using at least two criteria, namely both the *Q*-factor and the RMSD parameter to improve the reliability and relevance of results. This change of sign at one 6ex deuterium position can be explained by slight differences of orientation of the solute in the two types of samples (mono- and bimesophasic) and also by not strictly identical temperatures of samples in the field. Both effects can affect the relative position of some C-D vectors with respect to the axis defined by the magic angle (θ_m = 54.7°), up to the reversal of the sign of the $S_{C\text{-}D}$ parameter, and thus changing the sign of ^{2}H-RQC. However, it can be noted here that the calculated generalized degree of order (GDO) value (**Eq. SI-5**) and the eigenvalues as well, in both types of samples are in the same order of magnitude and rather close indicating that the interaction pattern between (D)-(+)-camphor and polypeptide and polyacetylene polymer remains close regardless of the sample type (see **Tables 1** and **SI-6**).[18] The excellent agreement between experimental and back-calculated data for each phase can also be assessed visually using comparative graphs as well as the correlation plots where the R^2 factor is equal to 0.999 in this example (see **Figure SI-10** and **SI-11**). The key order-based data for each domain are summarized in **Table 1**.

Table 1. Key Order-based data of (D)-(+)-camphor

Polymeric domain	L-MSP	PBLG
Conf. of the rep. unit	*S* / (L)	*S* / (L)
Polymer abs. conf.	*M*	*M*
Q-factor [a]	0.015	0.012
RMSD [b]	2.24	4.96
Eigenvalues of $S_{\alpha\beta}$	$S_{x'x'}$ = -2.41	$S_{x'x'}$ = -10.08
$S_{x'x'}$, $S_{y'y'}$, $S_{z'z'}$ ($\times 10^{-4}$)	$S_{y'y'}$ = -10.53	$S_{y'y'}$ = -27.64
	$S_{z'z'}$ = +12.94	$S_{z'z'}$ = +37.72
GDO ($\times 10^{-3}$) [c]	1.38	3.91
Axial comp. ($\times 10^{-3}$)	+1.29	+3.77
Rhombic comp. ($\times 10^{-3}$)	+0.54	+1.171
Rhombicity par. ($\times 10^{-1}$)	+4.19	+3.10
Asymmetric par. ($\times 10^{-1}$)	+6.28	+4.66
β angle [d]	47.9	
GCB [e]	0.67	

[a] Cornilescu's Factor of quality, *Q,* for the best-fit between experimental and back-calculated ^{2}H-RQC data (**Eq. SI-2**). [b] RMSD: standard root mean square deviation (**Eq**. **SI-3**). [c] GDO: generalized degree of order. [d] Value of generalized 9D-angle β between the Saupe matrices of **(D)-1** for the best-fit (**Eq. SI-6**). [e] GCB: Generalized cosine of 9D-angle "Cosine β".

As expected, the analysis of the results clearly shows two (linearly independent and uncorrelated) sets of ordering parameters with significant discrepancies in: i) the $S_{z'z'}$ parameter or the GDO value (**Eq. SI-5**), and ii) the intertensor generalized 9D-angle β (47.9°) (**Eq. SI-6**) or the GCB value (0.67) between the Saupe matrices, thus evidencing that **(D)-1** is aligned in average in a very different way in both chiral mesophases. These differences of molecular orientation due to differences in the polymer-solute interaction array can be visualized with the help of a graphical representation of camphor tensors in both domains (using 3D surfaces) as depicted in **Figure 5**.[24] Finally the difference of GCB value (0.67 *vs.* 0.80) calculated from the bimesophasic sample and the two monophasic samples (see **Table SI-6**) originates from small variations in the temperature and composition of samples.[18]

By providing two series of independent set of ^{2}H-RQCs, this new analytical approach paves the way for robust applications in 3D structure elucidation with increased reliability. Among potential new developments, we are exploring the possibility of combining the two sets of ^{2}H-RQC values to improve the reliability on the sign determination of RQCs in each mesophase. In addition, this exciting exploratory work opens up multiple promising practical developments (extraction of (^{13}C-^{1}H)-RDCs using ^{13}C 1D or 2D-NMR, extension to other polymeric mixtures giving rise to bimesophasic chiral systems), and associated applications (reliable comparative studies on enantiodiscrimination ability from a single oriented sample, measurement of two independent sets of RDCs or RCSAs). Another important aspect of future research on bimesophasic samples would be to exploit the thermoresponsiveness of the

system in order to control the orientational strength as well as the possible switching between isotropic and anisotropic states in each individual mesophase. In this case, the experimental determination of scalar couplings and the isotropic chemical shifts would be possible using a single NMR sample

Finally, the investigation of the demixing process and the understanding of the molecular parameters leading to stable bimesophasic systems also deserve special attention. All these aspects are currently the subject of in-depth research.

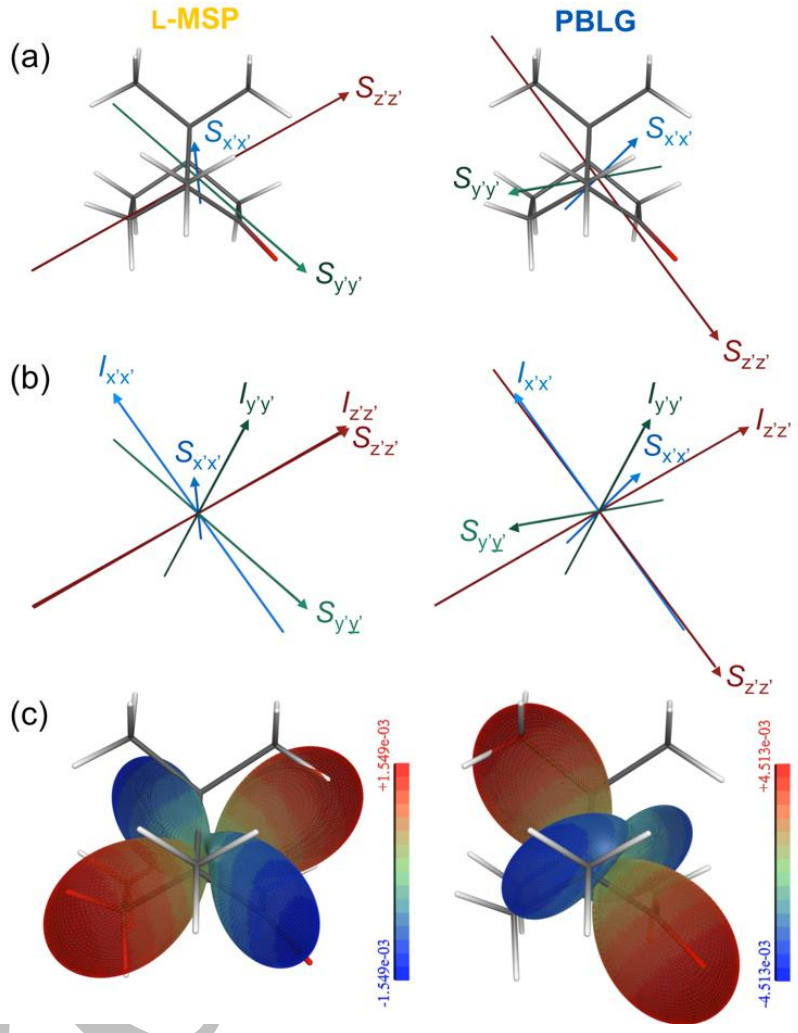

Figure 5. (a) Representation of the principal axis system ($S_{x'x'}$, $S_{y'y'}$, $S_{z'z}$) of the diagonalized Saupe matrix along the structure of **(D)-(1)** in L-MSP and PBLG domain. (b) Comparison of the principal axis system ($S_{x'x'}$, $S_{y'y'}$, $S_{z'z'}$) and the inertia tensor axe ($I_{x'x'}$, $I_{y'y'}$, $I_{z'z'}$). (c) Visualization of the alignment tensors as a 3D surface. Blue colour codes for negative and red for positive values. Color scaling is adapted to the maximum scaling of the ^{2}H-RQCs in the corresponding directions for vectors pointing from the center of the tensor plot to the individual surface points.

ASSOCIATED CONTENT:

Supporting Information

In Supporting information (PDF file) is given: i) a brief description of structure elucidation; ii) the composition of samples; iii) supplementary isotropic and anisotropic NMR spectra; iv) atomic coordinates of **(D)-1**.

AUTHOR INFORMATION:

Notes

The authors declare no competing financial interests.

ACKNOWLEDGMENTS:

French authors thank CNRS and Paris-Saclay University for recurrent funding. Financial support provided by the DFG (Re 1007/9-1 / CAPES 418729698) is gratefully acknowledged by the german contributors. P.L. would also like to thank the Ile-de-France region (SESAME project), French MESR and CNRS Chimie and all Paris-Saclay partners for providing funding for new NMR equipment.

REFERENCES:

(1) Lesot, P.; Aroulanda, C.; Berdagué P.; Meddour, A.; Merlet, D.; Farjon, J.; Giraud, N. Lafon, O.; NMR in polypeptide liquid crystals: three fertile decades of methodological developments and analytical challenges. *Prog. Nucl. Magn. Reson. Spectrosc*. **2020**, *116,* 85–154.

(2) Lesot, P.; Gil, R. R.; Anisotropic 1D/2D NMR in molecular analysis, *in two dimensional (2D) NMR methods*, (**2023**). Chap. IX, Eds. Ivanov, K.; Madhu, P. K.; Rajalakshmi, G.; DOI: 10.1002/ 97811 19806721.ch9.

(3) Li, G.W.; Liu, H.; Qiu F.; Wang, X.-J.; Lei, X.-X.; Residual dipolar couplings in structure determination of natural products. *Nat. Prod. Bioprospect*. **2018**, *8*, 279–295.

(4) Li, X.; Yang, X.; Sun. H.; NMR for stereochemical elucidation in *Chiral Separations and Stereochemical Elucidation*, Wiley (**2023**), Chap. 13, Eds. Bezerra Cass, Q.; Tiritan, M. E.; Batista, J. M.; Jr; Barreiro, J.C.

(5) Lesot, P.; Gil, R. R.; Berdagué, P.; Navarro-Vázquez, A.; Deuterium residual quadrupolar couplings: crossing the current frontiers in the relative configuration analysis of natural products. *J. Nat. Prod*. **2020**, *83*, 3141–3148.

(6) Navarro-Vázquez, A.; Berdagué, P.; Lesot, P.; Integrated computational protocol for the analysis of quadrupolar splittings from natural-abundance deuterium NMR spectra in (chiral) oriented media. *J. Nat. Prod.* **2017**, *18*, 1252–1266.

(7) Immel, S.; Köck, M.; Reggelin, M.; NMR-based configurational assignments of natural products: how floating chirality distance geometry calculations simplify gambling with 2^{n-1} diastereomers. *J. Nat. Prod.* **2022**, *85*, 1837–1849.

(8) Qin, S.-Y.; Jiang, Y.; Sun, H.; Liu, H.; Zhang, A.-Q.; Lei, Xi.; Measurement of residual dipolar couplings of organic molecules in multiple solvent systems using a liquid crystalline based medium. *Angew. Chem. Int. Ed.* **2020**, *132*, 17245–17251.

(9) Köck, M.; Reggelin, M.; Immel, S.; The advanced floating chirality distance geometry approach-how anisotropic NMR parameters can support the determination of the relative configuration of natural products. *Mar. Drugs* **2020**, *18*, 330, (1-22).

(10) Roth, F. A.; Schmidts, V.; Thiele, C.-M.; TITANIA: Model-free interpretation of residual dipolar couplings in the context of organic compounds. *J. Org. Chem.* **2021**, *86*, 15387–15402.

(11) Sager, E.; Tzvetkova, P.; Gossert, A. D.; Piechon, P.; Luy, B.; Configurational analysis by residual dipolar coupling driven floating chirality distance geometry calculations. *Chem. Eur. J.* **2020**, *26*, 14435–14444.

(12) Liu, Y.; Navarro-Vazquez, A.; Gil, R. R.; Martin, G. E.; Williamson, R. T.; Application of anisotropic NMR parameters to the confirmation of molecular structure. *Nature Protocols* **2019**, *14*, 217–249.

(13) Immel, S.; Köck, M.; Reggelin, M.; Configurational analysis by residual dipolar coupling driven floating chirality distance geometry calculations. *Chem. Eur. J.* **2018**, *24*, 13918–13930.

(14) Immel, S.; Köck, M.; Reggelin, M. Bayesian inference applied to NMR-based configurational assignments by floating chirality distance geometry calculations. *J. Am. Chem. Soc.* **2022**, *144*, 6830–6838.

(15) Schirra, D. S.; Hirschmann, I. M.; Radulov, A.; Lehmann, M.; Thiele, C.-M.; Investigations of the alignment process of homopolyglutamate based LLC phases: Deuterium NMR analysis of PBPMLG reveals a 90° flip of the polymer. *Angew. Chem. Int. Ed.* **2021**, *60*, 21040–21046.

(16) Schwab, M.; Schmidts, V.; Thiele, C.-M.; Polyaspartates as thermoresponsive enantiodifferentiating helically chiral alignment media for anisotropic NMR spectroscopy. *Chem. Eur. J.* **2018**, *24*, 14373–14377.

(17) Geckeler, K. E.; Rupp, F.; Geis-Gerstorfer, J.; Interfaces and interphases of (bio)materials. *Adv. Mater.* **1997**, *9*, 513–518.

(18) Berdagué, P.; Gouilleux, B.; Noll, M.; Immel, S.; Reggelin, M.; Lesot, P.; Study and quantification of the enantiodiscrimination power of four polymeric chiral LLCs using NAD 2D-NMR. *Phys. Chem. Chem. Phys.* **2022**, *24*, 7338–7348.

(19) Trigo-Mouriño, P.; Merle, C.; Koos, M. R. M.; Luy, B.; Gil R. R.; Probing spatial distribution of alignment by deuterium NMR imaging. *Chem. Eur. J.* **2013**, *19*, 7013–7019.

(20) Dumez, J.-N.; Spatial encoding and spatial selection methods in high-resolution NMR spectroscopy. *Prog. Nucl. Magn. Reson. Spectrosc.* **2018**, *109*, 101–134.

(21) Jézéquel, T.; Silvestre, V.; Dinis, K.; Giraudeau, P.; Akoka, S.; Optimized slice-selective ^{1}H NMR experiments combined with highly accurate quantitative ^{13}C NMR using an internal reference method. *J. Magn. Reson.* **2018**, *289*, 18–25.

(22) Mitrev, Y. N.; Slice selective NMR approach for investigation of distribution phenomena in biphasic samples. *Bulg. Chem. Commun.* **2017**, *49*, 65–69.

(23) Navarro-Vázquez, A.; MSpin-RDC. A program for the use of residual dipolar couplings for structure elucidation of small molecules. *Magn. Reson. Chem.* **2012**, *50*, S73–S79.

(24) Kramer, F.; Deshmukh, M. V.; Kessler, H.; Glaser, S. J.; Residual dipolar coupling constants: an elementary derivation of key equations. *Concept of Magn. Reson. A*. **2004**, *21A*, 10–21.